Instability and sensitivity analysis of streaming nanofluid-air interface

Rishi Asthana [a], Ziya Uddin [a, *], Mukesh Kumar Awasthi [b], Arpit Bhardwaj [c], Wubshet Ibrahim [d]

[a] *School of Engineering & Technology, BML Munjal University, Gurgaon, Haryana, India*
[b] *Department of Mathematics, Babasaheb Bhimrao Ambedkar University, Lucknow, India*
[c] *School of Computer Science Engineering and Technology, Bennett University, Greater Noida, UP, India*
[d] *Department of Mathematics, Ambo University, Ambo, Ethiopia*

Abstract

The nanofluid/air interface is practically used in enhancing heat transfer efficiency in thermal management systems, such as in cooling electronics and improving the performance of solar collectors. Additionally, it finds applications in advanced manufacturing processes and biomedical devices, where precise temperature control is crucial. The study investigates the instability of the interface between a Newtonian nanofluid and air in a rectangular setup. This instability arises when the two fluids flow at different velocities, leading to Kelvin-Helmholtz instability at the interface. The air is treated as a viscous, incompressible fluid due to its low Mach number, positioned above the nanofluid. The stability of the interface is determined based on the relative velocity of the fluid layers. The study reveals that various flow parameters, including viscosity ratio, density ratio, volume fraction, and nanoparticle diameter, influence the stability or instability of the interface. Four types of nanofluids are considered, and a comparative analysis is conducted. Interestingly, the nanofluid/air system is found to be more stable compared to the viscous liquid/air system. Sensitivity analysis is performed to examine the impact of different physical variables and their interactions on the critical relative velocity. It is observed that the critical velocity consistently exhibits positive sensitivity to the density ratio. Moreover, the magnitude of critical velocity sensitivities for the density ratio remains constant across all cases. The critical velocity demonstrates the highest positive sensitivity with respect to the parameter of air thickness, with this maximum sensitivity occurring when the air thickness equals 1 and the densities of both fluids are identical.

Keywords: Nanofluids; Kelvin-Helmholtz instability; Brownian motion; Normal-mode analysis; Sensitivity Analysis

1. Introduction

The interface of two distinct fluids may be unstable if a velocity difference occurs at the interface. This velocity difference causes fluctuations in pressure, which trigger the instability. This phenomenon was observed

---

* Corresponding author. ziyauddin1982@gmail.com

by Helmholtz [1] in the flow field, and Thomson [2] provided a mathematical description of it. As a result, this instability is known as Kelvin-Helmholtz instability (KHI). KHI is commonly observed in various natural and industrial scenarios, such as when air blows over mercury, during the entry of meteors into Earth's atmosphere, and in the swirling movement of ionized bolides in air purifiers, among others.

Drazin [3] conducted a study on the Kelvin-Helmholtz instability, where the fluids were assumed to be non-viscous and the flows were considered non-rotational. In this analysis, the flow field was left unrestricted so that disturbances would decay far from the interface. Maslowe and Kelly [4] utilized the power-series expansion method to investigate the finite amplitude periodic interfacial waves of two incompressible fluids. Nayfeh and Saric [5] conducted a nonlinear analysis to study the stability of a liquid film neighboring a compressible gas, considering the effect of body force directed either externally from or in the direction of the liquid. Weissmann [6] examined the interfacial instability between two streaming semi-infinite fluids and derived time-dependent first and second-order equations. It's worth noting that these studies were limited to inviscid fluids.

In fluid dynamics, if the motion of a fluid is irrotational, it means that the fluid particles don't rotate as they move. Joseph and Liao [7] proposed a theory called VPF (viscous potential flow) theory, which analyzes irrotational fluid flow even when there's viscosity involved. This theory includes viscosity in the dynamical equation at the interface. Funada and Joseph [8] further explored the Kelvin-Helmholtz instability (KHI) for two viscous fluids in a horizontal rectangular channel. Although their study was inspired by the work of Drazin, they considered viscosity to be present. Awasthi and Agrawal [9] investigated KHI at a cylindrical interface. Their findings were similar to those of Funada and Joseph for plane geometry, but they discovered that cylindrical geometry was less stable than planar geometry. Kim et al. [10] conducted a comparison of KHI using four different theories and found that the dissipation method predicts the most stable interface among them. Various authors [11-13] applied VPF theory to examine KHI at the interface of two Newtonian/non-Newtonian fluids.

The physical properties of liquids such as viscosity, conductivity, density, etc. play a significant impact in the phenomenon of stability of ordinary liquids; these properties remain the same over a particular range of temperatures. Therefore, to improve the stabilization of the flow either the fluid has to be changed or the channel should be changed. Since flow stability has so many practical and natural applications, it is not possible to change the channel as well as the fluid flowing through the channel. Therefore, if the physical properties of the pure liquid can be changed by using some additives, the stabilization phenomenon can be modified. In comparison to ordinary fluids, the metal density and metal oxide densities are very high and therefore, the physical properties of an ordinary fluid can be revised by adding metal oxide/metal particles into it. The inclusion of nano-sized metal-oxide/metal particles into an ordinary fluid makes the nanofluids. The applications of nanofluids in various industries through their physical properties were examined by various authors [14-18]. They established that the physical variables of a nanofluid significantly depend on the size and shape of suspended metal nanoparticles, the physical and thermal properties of the nanoparticles, the nanoparticle concentration, and the base fluid. It was shown by Gaganpreet and Srivastava [19] that the nanofluids viscosity depends upon the shape and size of the interfacial layer of the dispersed nano-sized metal oxide/metal nanoparticles.

Nanofluids have vast industrial applications such as microelectronics, automobiles, nano-chips, etc. and therefore, it has attracted numerous researchers working in the field of stability of fluid flow. Moatimid and Hassan [20] analyzed the linear convection instability of the viscoelastic nano-fluid of Walter's type along with a vertical layer. The stability of two electrically conducting nano-fluid layers was made by Moatimid and Gaber [21]. They consider two combinations for their study namely; water Al_2O_3 −oil CuO nanofluid and water Al_2O_3 −oil TiO_2 nanofluid. They consider the effect of temperature difference at the basic state and found that the increase in temperature difference has a destabilizing effect. Ahuja and Girotra [22] studied RTI in nanofluids numerically as well as analytically. Awasthi et al. [23] examine the temporal instability of the interface between a power-low viscoelastic nanofluid and a viscous fluid. Girotra et al. [24] added rotational effects on the RTI of the nanofluids interface. The RTI of nanofluids in a porous medium was analytically analyzed by Ahuja and Girotra [25]. Awasthi et al. [26] examine the RTI at the interface of nanofluid in a circular geometry. The interface of a nanofluid film in a cylindrical configuration with heat transport was considered by Motaimid et al. [27]. Han [28] considered the temperature and concentration effects on the KHI of a nanofluid layer. He also included the Marangoni effect. The instability of nanofluid-viscous fluid in a circular cavity was examined by Awasthi et al. [29]. The spherical interface of nanofluid-viscous fluid was studied by Agarwal et al. [30].

The study of the division of uncertainty into the output of a mathematical model or system is called sensitivity analysis. Through this analysis, one can also find the allocation of various sources of uncertainty. It can also be referred to as a simulation mechanism or 'what-if'. The method of redirecting a given decision by a certain category also comes under sensitivity analysis. An analyst, by aggregating all the variables, can also know how changes in one variable can affect the result. Leonzio and Zondervan [31] analyzed the absorption process of CO2 from gas with ionic fluid statistically. The sensitivity analysis of MHD nanofluid flow with MWCNTs containing engine

oil over a disk with rotation was established by Mehmood et al.[32]. They reported that if the nanoparticle's volume fraction increases, the fluid velocity deteriorates. Other recent works on the sensitivity analysis of sisko nanofluid flow and hybrid nanofluid flow were investigated by Upreti et al. [33] and Uddin et al. [34], respectively. Beg et al. [35] conducted an experimental investigation into the lubricity and rheology properties of a drilling fluid, driven by its potential applications in extended reach wells. Shamshuddin et al. [36] made a significant contribution by thoroughly examining the heat and mass transfer phenomena in the NF ND–Cu/H₂O system, specifically under the effect of an exponentially stretching velocity. Salawu et al. [37] conducted a study on the hybridization of zirconium dioxide and copper tangent hyperbolic nanofluid in an ethylene glycol (EG) solvent to optimize thermal power.

The sensitivity analysis of an unstable interface involving moving fluids has not yet been thoroughly investigated in academic research. This paper addresses the stability of the plane interface formed between a viscous fluid and a Newtonian nanofluid. Using the Response Surface Method (RSM), we perform a sensitivity analysis of the nanofluid/air interface. The fluids flow at different velocities, causing the interface to experience Kelvin-Helmholtz Instability (KHI).

Funada and Joseph [8] studied the stability of a pure water-air interface without addressing the sensitivity of any parameters. In contrast, this study focuses on the stability of the nanofluid-air interface and includes a comprehensive sensitivity analysis of various parameters affecting the system's stability. We utilize a planar coordinate system (x, y, z) to formulate the mathematical governing equations. The irrotational theory of viscous fluids is employed to solve the linear perturbed equations. Applying the normal mode procedure, a second-order polynomial based on the perturbation's growth parameter is derived through a linear stability analysis. Our analysis successfully recovers the dispersion relation of Funada and Joseph [8] for the corresponding Newtonian fluid.

The paper is organized as follows: Section 2 presents the modeling of the physical problem, including differential equations and the necessary boundary and interfacial conditions. In Section 3, the perturbation is applied, resulting in the derivation of linear equations. The relationship between the growth parameter and wave number, derived through linear stability analysis, is also included in this section. Section 4 discusses the numerical computation and sensitivity analysis. Finally, Section 5 outlines the key results of the study.

2. Mathematical Modeling

Consider an interface $y = 0$ (figure 1) that separates the Newtonian nanofluid and air in a rectangular channel. Both the nanofluid and the air are assumed to be incompressible and viscous fluids, and the depth of the channel is finite. Specifically, the nanofluid occupies the lower portion of the channel, while the air is located in the upper region. The nanofluid has density ρ_{nf}, viscosity μ_{nf} and depth h_{nf} while air has respective parameters are ρ_2, μ_2 and h_2. Accepting the formulation given by Ziya et al.[15], the nanofluid density, in terms of nanoparticles volume fraction ϕ, base fluid density ρ_f, and metal particle density ρ_p defined as

$$\rho_{nf} = \phi\rho_p + (1-\phi)\rho_f \tag{1}$$

The nanofluid's viscosity is a function of base fluid viscosity, volume fraction of nanoparticles, shape of the metal nanoparticles, and the nano-layer formed around the nanoparticles by fluid elements. Considering the impact of the above parameters, the mathematical expression of nanofluid viscosity μ_{nf} can be written as (Gaganpreet et al. [19])

$$\mu_{nf} = \mu_f \left(1 - \frac{\phi_{ag}}{\phi_m}\right)^{-[\delta]\phi_m} \tag{2}$$

In the above expression, μ_f denotes the base fluid viscosity. The nanoparticles shape parameter is denoted by δ and for sphere-shaped nanoparticles $\delta = 2.5$. Here it is assumed that the nanoparticles are swirling about their axes and therefore prolate spheroids shape nanoparticles considered here. In equation (2), the term ϕ_m represents the prolate spheroid's maximum volume fraction and it was shown through various experiments that $0.68 \leq \phi_m \leq 0.74$. In the present analysis, ϕ_m is taken as 0.74. The term ϕ_{ag} denotes aggregate volume fraction which is related to the equivalent volume fraction ϕ_{mod} with fractal index d as

$$\phi_{ag} = \phi_{mod}\left(\frac{r_a}{r}\right)^{3-d}$$ (3)

The relation of ϕ_{mod} and ϕ can be expressed in terms of interfacial layer thickness γ, semi-minor axis length b, and semi-major axis length a of nanoparticles as follows

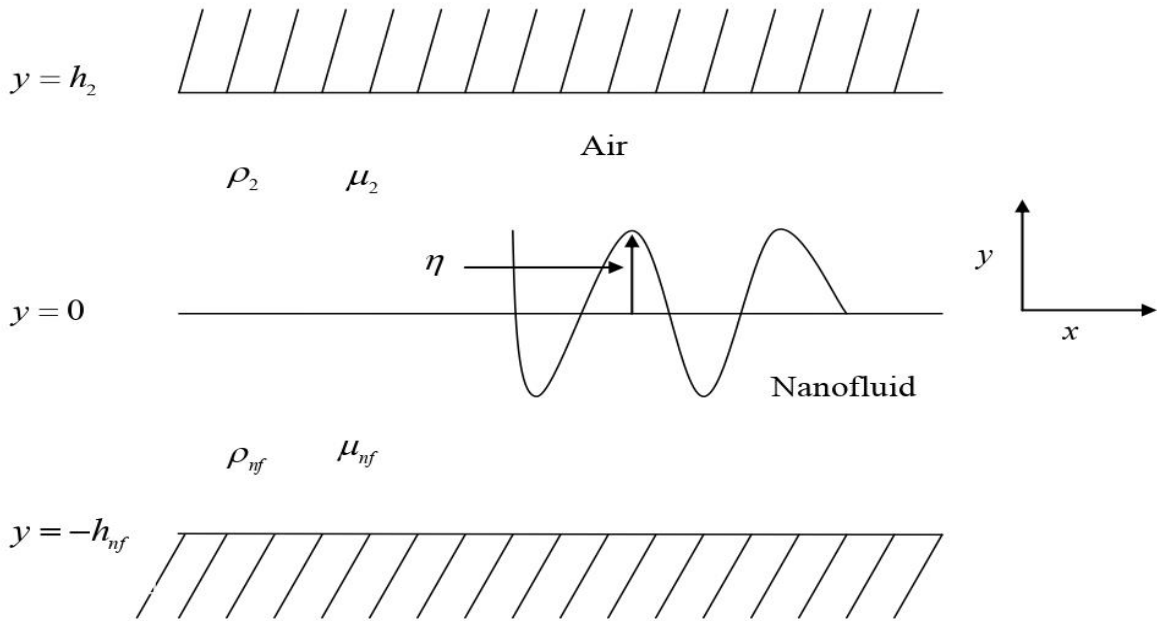$$\phi_{mod} = \phi\left(1+\frac{\gamma}{a}\right)\left(1+\frac{\gamma}{b}\right)^2$$ (4)

Figure 1: Schematic diagram of the problem.

The mathematical governing equations for fluid phases can be written as (Awasthi et al. [23])

$$\nabla \cdot \vec{q}_{nf} = 0$$
$$\left.\frac{\partial \vec{q}_{nf}}{\partial t} + \left(\vec{q}_{nf} \cdot \nabla\right)\vec{q}_{nf} = -\frac{1}{\rho_{nf}}\nabla p_{nf} + \vec{g} + v_{nf}\nabla^2\vec{q}_{nf}\right\}$$ (5)

$$\nabla \cdot \vec{q}_2 = 0$$
$$\left.\frac{\partial \vec{q}_2}{\partial t} + \left(\vec{q}_2 \cdot \nabla\right)\vec{q}_2 = -\frac{1}{\rho_2}\nabla p_2 + \vec{g} + v_2\nabla^2\vec{q}_2\right\}$$ (6)

Here, $\vec{q}_{nf} = (u_{nf}, v_{nf})$ and $\vec{q}_2 = (u_2, v_2)$ are the velocities in the nanofluid phase and viscous fluid phase, respectively. The gravitational acceleration is represented by $\vec{g}$ and p_{nf}, p_2 are the pressures in the nanofluid and air phases, respectively.

2.1. Boundary conditions

The boundaries $y = -h_{nf}$ and $y = h_2$ are rigid and therefore there is no flow across them (Awasthi et al.

[23]).

$$v_{nf} = 0 \quad \text{at} \quad y = -h_{nf}$$

$$v_2 = 0 \quad \text{at} \quad y = h_2$$

(7)

2.2. Interfacial conditions

At the free surface, the normal component of interfacial velocity will be zero, and therefore,

$$\frac{\partial E}{\partial t} + \vec{q}_{nf} \cdot \nabla E = 0$$

$$\frac{\partial E}{\partial t} + \vec{q}_2 \cdot \nabla E = 0$$

(8)

Here $E = E(x, y, t)$ represents the interface equation.

The surface tension force will neutralize the difference between normal stresses at the free surface. This condition is called the dynamical interface condition. Mathematically (Awasthi et al. [23]),

$$(p_2 - \hat{n} \cdot \tau_2) - (p_{nf} - \hat{n} \cdot \tau_{nf}) = -\sigma \nabla \cdot \hat{n}$$

(9)

Here, τ_2, τ_{nf} denote normal viscous stresses in air and nanofluid phase, respectively. σ represents surface tension while $\hat{n}$ indicates unit outward normal at the interface.

Initially, the undisturbed interface between two fluid layers is at $y = 0$. In this state, $\vec{q}_{nf} = (U_{nf}, 0)$ and $\vec{q}_2 = (U_2, 0)$ where U_{nf} and U_2 are constant velocities and therefore $p_{nf} = \text{constant} = p_2$.

The stability of the plane interface is examined in the sense that whether a perturbation of small amplitude at the interface grows diminishes. Imposing perturbation, the interface takes the form as

$$E(x, y, t) = y - \eta(x, t) = 0.$$

(10)

Here, $\eta(x, t)$ denotes interface elevation. The outward unit normal to the first-order term is given by

$$\hat{n} = (-\eta_x \hat{i} + \hat{j})$$

(11)

In the perturbed state, the velocity of the nanofluid phase $\vec{q}_{nf} = (U_{nf} + u'_{nf}, v'_{nf})$ and the velocity of the viscous fluid phase $\vec{q}_2 = (U_2 + u'_2, v'_2)$. Since the perturbed flow is taken as irrotational here, there exist potential functions ϕ_{nf} for nanofluid and ϕ_2 for viscous fluid which satisfies the Laplace equation i.e.

$$\nabla^2 \phi_{nf} = 0$$

(12)

$$\nabla^2 \phi_2 = 0$$

(13)

The normal mode procedure is applied to study the stability of the plane interface. The interface elevation is expressed as $\eta(x, t) = e^{-i\omega t} E e^{ikx}$ and perturbed quantities $F'(x, y, t) = e^{-i\omega t} F(y) e^{ikx}$. Here, ω denotes growth rate parameter

while k represents wavenumber, E is a constant.

In the perturbed state, the linear form of equation (8) at $y = 0$ can be written as

$$\frac{\partial \eta}{\partial t} + U_{nf}\frac{\partial \eta}{\partial x} = \frac{\partial \phi_{nf}}{\partial y}$$

$$\frac{\partial \eta}{\partial t} + U_{2}\frac{\partial \eta}{\partial x} = \frac{\partial \phi_{2}}{\partial y} \tag{14}$$

3. Dispersion relationship

Hence the expression of ϕ_{nf} and ϕ_{2} are

$$\phi_{nf} = \frac{1}{k}(ikU_{nf} - i\omega)e^{-i\omega t}E\frac{\cosh(k(y + h_{nf}))}{\sinh kh_{nf}}e^{ikx} \tag{15}$$

$$\phi_{2} = -\frac{1}{k}(ikU_{2} - i\omega)e^{-i\omega t}E\frac{\cosh(k(y - h_{2}))}{\sinh kh_{2}}e^{ikx} \tag{16}$$

The linear dynamical equation in a perturbed state can be achieved as

$$\left(p_{nf} - p_{2}\right) - 2\left(\mu_{f}\left(1 - \frac{\phi_{ag}}{\phi_{m}}\right)^{-[\delta]\phi_{m}}\frac{\partial^{2}\phi_{nf}}{\partial y^{2}} - 2\mu_{2}\frac{\partial^{2}\phi_{2}}{\partial y^{2}}\right) = \sigma\frac{\partial^{2}\eta}{\partial x^{2}} \tag{17}$$

Bernoulli's equation is employed to compute the pressures in equation (17) and therefore, it reduces to

$$\left[\rho_{2}\left(\frac{\partial \phi_{2}}{\partial t} + g\eta + U_{2}\frac{\partial \phi_{2}}{\partial x} + 2\mu_{2}\frac{\partial^{2}\phi_{2}}{\partial y^{2}}\right)\right] - \left[\rho_{nf}\left(\frac{\partial \phi_{nf}}{\partial t} + g\eta + U_{nf}\frac{\partial \phi_{nf}}{\partial x}\right) + 2\mu_{f}\left(1 - \frac{\phi_{ag}}{\phi_{m}}\right)^{-[\delta]\phi_{m}}\frac{\partial^{2}\phi_{nf}}{\partial y^{2}}\right] = -\sigma\frac{\partial^{2}\eta}{\partial x^{2}} \tag{18}$$

Putting the expressions of η, Φ_{nf} and Φ_{2} to the equation (18), the relation is achieved as

$$A_{o}\omega^{2} + \left(A_{1} + iB_{1}\right)\omega + \left(A_{2} + iB_{2}\right) = 0 \tag{19}$$

Where

$$A_{0} = \rho_{nf}\coth kh_{nf} + \rho_{2}\coth kh_{2}$$

$$A_{1} = -2k\left(\rho_{nf}U_{nf}\coth kh_{nf} + \rho_{2}U_{2}\coth kh_{2}\right)$$

$$B_{1} = 2k^{3}(\mu_{nf}\coth kh_{nf}f + \mu_{2}\coth kh_{2})$$

$$A_{2} = k^{2}\left(\rho_{nf}U_{nf}^{2}\coth kh_{nf} + \rho_{2}U_{2}^{2}\coth kh_{2}\right) + \left(\rho_{2} - \rho_{nf}\right)gk - \sigma k^{3}$$

$$B_2 = -2k^3\left(\mu_{nf} U_{nf} \coth kh_{nf} + \mu_2 U_2 \coth kh_2\right)$$

In equation (18) replacing ω by $i\omega$, the relation given by Funada and Joseph [8] is achieved.

Equation (19) may be re-written as

$$\omega^2 + 2(p+iq)\omega + c + 2ic_1 = 0;$$

$$p = \frac{A_1}{2A_0}, q = \frac{B_1}{2A_0}, c = \frac{A_2}{A_0}, c_1 = \frac{B_2}{2A_0} \tag{20}$$

The perturbation's growth is a complex quantity i.e. $\omega = \omega_R + i\omega_I$.. Equation (20) can be separated into real and imaginary parts as

$$\left.\begin{array}{l} \omega_R \omega_I + p\omega_I + q\omega_R + c_1 = 0 \\ \omega_I^2 - \omega_R^2 + 2q\omega_I - 2p\omega_R - c = 0 \end{array}\right\} \tag{21}$$

Substitute

$$\omega_I = -\zeta\sqrt{pq} - q, \quad \omega_R = \eta\sqrt{pq} - p$$

Then (20)

$$\left\{\begin{array}{l} \xi\eta = C_1 \\ \xi^2 - \eta^2 = 2C. \end{array}\right. \tag{22}$$

Where

$$C = \frac{c - p^2 + q^2}{2pq}, C_1 = -1 + \frac{c_1}{pq} \tag{23}$$

We found a biquadratic equation in ζ as

$$\zeta^4 - 2C\zeta^2 - C_1^2 = 0 \tag{24}$$

$$\zeta_{1,2} = \sqrt{C \pm \sqrt{C^2 + C_1^2}} \tag{25}$$

Then the decrement instability will look like

$$\left(\omega_I\right)_{1,2} = -\zeta_{1,2}\sqrt{pq} - q \tag{26}$$

From equation (26), the wave growth parameter can be obtained as a function of wave number. it is well-known fact that for neutral stability $\omega_I = 0$ and therefore the neutral stability curves can be achieved by the expression $\zeta_{1,2}\sqrt{pq} = -q$ i.e. $\zeta^2 = \dfrac{q}{p}$, which in turn implies that

$$q^2 c - 2c_1 pq + c_1^2 = 0 \tag{27}$$

Eliminating p, q, c, c_1 into the above equation, the expression of the relative velocity $V = U_2 - U_{nf}$ is achieved as

$$V^2 = \frac{1}{k} \frac{\left[\left(\rho_{nf} - \rho_2\right)g + \sigma k^2\right]\left[\mu_{nf}\coth kh_{nf} + \mu_2\coth kh_2\right]^2}{\left[\rho_{nf}\mu_{nf}^2\coth kh_{nf}\coth^2 kh_2 + \rho_2\mu_2^2\coth^2 kh_{nf}\coth kh_2\right]} \tag{28}$$

The lowest point on the curves $V^2(k)$ is obtained as

$$V_c^2 \equiv V^2(k_c) = \min_{k \geq 0} V^2(k) \tag{29}$$

The flow is unstable if

$$V^2 = (-V)^2 > V_c^2. \tag{30}$$

Take $H = h_1 + h_2$ as characteristic length and

$$\hat{k} = kH, \hat{h}_1 = \frac{h_1}{H}, \hat{h}_2 = \frac{h_2}{H}, \hat{\rho} = \frac{\rho_2}{\rho_f}, \hat{\mu} = \frac{\mu_2}{\mu_f}, \hat{V} = \frac{V}{Q}, \hat{\sigma} = \frac{\sigma}{\rho_f g H^2}, \quad \text{and}$$

$$Q = \left[\frac{(1 - \hat{\rho}) gH}{\hat{\rho}}\right]^{\frac{1}{2}}$$

The dimensionless form of equation (28) is given as

$$\hat{V}^2 = \frac{\left[A\tanh(\widehat{kh}_2) + \hat{\mu}\tanh(\widehat{kh}_1)\right]^2}{\left[A^2\tanh(\widehat{kh}_2) + B\left(\frac{\hat{\mu}^2}{\hat{\rho}}\right)\tanh(\widehat{kh}_1)\right]} \frac{1}{\hat{k}}\left[\frac{(B - \hat{\rho})}{(1 - \hat{\rho})} + \frac{\hat{\sigma}\hat{k}^2}{(1 - \hat{\rho})}\right] \tag{31}$$

Here $A = \left[1 - \dfrac{\phi_{ag}}{\phi_m}\right]^{-[\delta]\phi_m}$ and $B = \phi\hat{\rho}_p + (1 - \phi)$, $\hat{\rho}_p = \dfrac{\rho_p}{\rho_f}$

In the case of $A = 1$ and $B = 1$, equation (30) reduces to the same expression as achieved by Funada and Joseph [8].

4. Results and Discussions

4.1. Stability Analysis

This study carried out the numerical computation for four different types of nanofluids viz. $Al_2O_3 + H_2O$, $CuO + H_2O$, $Al_2O_3 + EG$ (ethylene glycol), and $CuO + EG$ with different nanoparticle concentrations. The viscosity model used for the calculations is validated from the published literature [19]. To compute the results the computer codes were written in MATLAB. Sphere-shaped particles have been considered for the calculation, therefore the value of δ is fixed at 2.5 and the value of fractal index parameter d is taken as 1.8. Other physical properties of the nanoparticles and the base fluids are the following:

$$\gamma = 2 \times 10^{-9}, a = b = r = 15 \times 10^{-9}, \rho_2 = 1.2, \mu_2 = 0.000018, \rho_{H_2O} = 1000, \mu_{H_2O} = 0.001,$$

$$\rho_{EG} = 1112.5, \mu_{EG} = 0.0283, \rho_{Al_2O_3} = 3880, \rho_{CuO} = 4230, \mu_{EG} = 0.0283,$$

$$s_{water\&air} = 0.06, \ s_{EG\&air} = 0.0473.$$
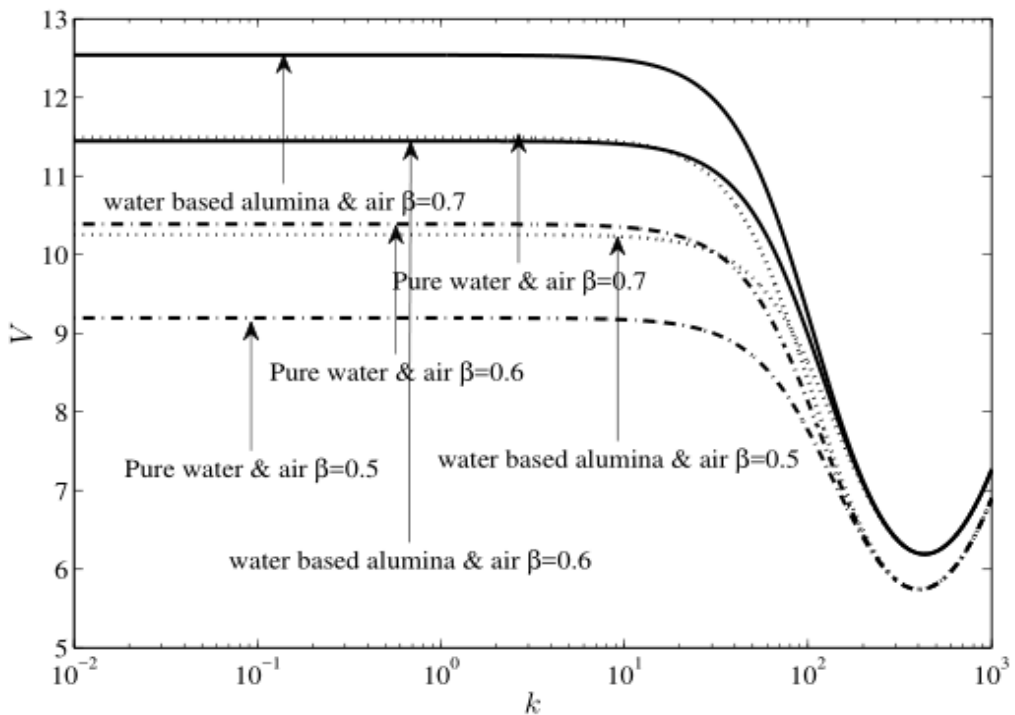
Figure 2: Comparison of water & air and water-based alumina $\varphi = 0.5$

In Figure 2, a comparison between two cases of fluid layers viz. pure water & air versus water-based alumina nanofluid & air for different upper fluid (Air) fractions have been made. It is observed that Nano fluid & Air is more stable than Water & Air combination for the same upper fluid fraction. With the increase in the value of the upper fluid fraction stability region also increases. The minimum values of wave number and corresponding minimum relative velocities for each of these neutral curves have been tabulated in table 1.

Table 1: Minimum relative velocity and wave number.

Fluid type	Upper fluid fraction β	Min k (1/m)	Min V (m/sec)

Water & Air (Funada and Joseph[8])	0.5	403.1	5.741
Water-based Alumina & Air	0.5	424.6	6.19
Water & Air	0.6	407.5	5.7412
Water-based Alumina & Air	0.6	425.6	6.19
Water & Air	0.7	407.5	5.743
Water-based Alumina & Air	0.7	425.6	6.19

In Figure 3, a comparison among pure water &air, water-based alumina (Al_2O_3), and cupric oxide (CuO) nanofluids has been made. The interface of pure water& air has already been discussed by Funada and Joseph [8]. It is depicted from the figure that the insertion of nano-sized particles in pure water stabilizes the flow behavior. The reason for this is the dependence of nanofluid viscosity on the density of nanoparticles. As given in the literature survey and equation (2), the viscosity of the nanofluid increases with the insertion of nanoparticles in pure fluid (water). It is also observed from the same figure that a water-based CuO nano fluid &air combination is more stable than water-basedAl_2O_3 nanofluid & Air.
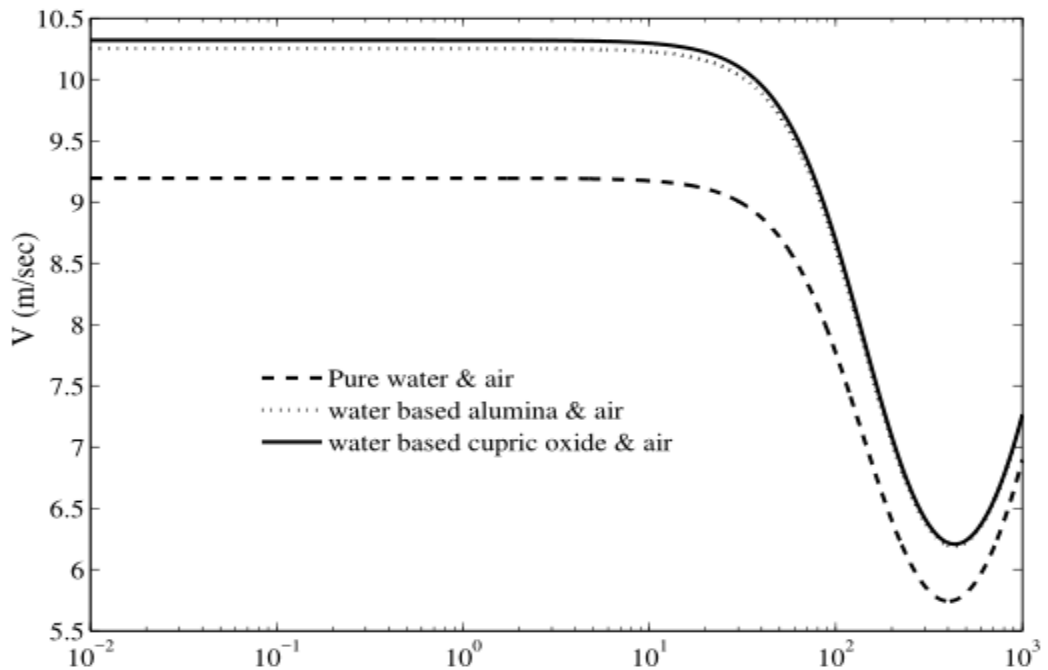

Figure 3: Comparison of pure water &air, water-based alumina, and water-based cupric oxide $\beta = 0.5, \varphi = 0.5$
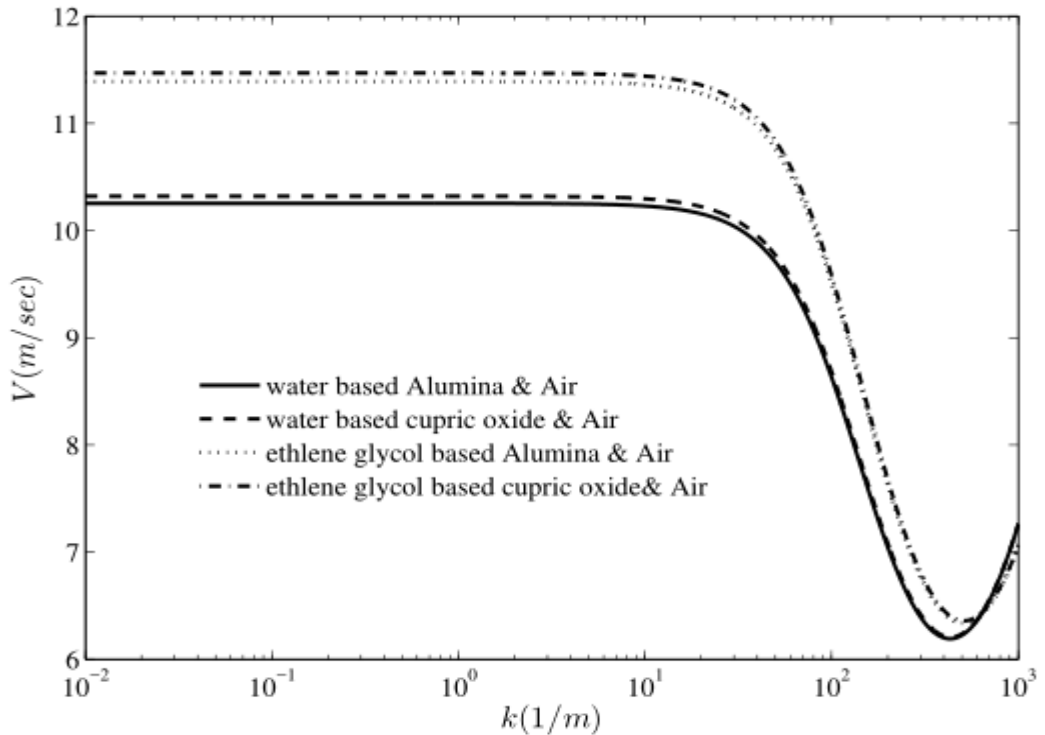
Figure 4: Comparison of water and eg-based nanofluids $\beta = 0.5, \varphi = 0.5$

Figure 4 shows the comparative stabilizing behavior for different nanofluids viz. water and ethylene glycol (EG) based Al_2O_3 and CuO nanofluids with air. It is observed that $CuO - EG$&air combination is the most stable among all combinations. In the previous figure, it was observed that CuO −water with air is more stable than Al_2O_3 − water &air. This means that the stabilizing behavior depends upon both the nanoparticle and the base fluid. The higher the density of nanoparticles and the more viscosity of base fluid results in more stable flow behavior. From the figure, it is also depicted that the flow stability behavior is reversed for large wave numbers. The reason for this reversal might be the increasing Brownian motion of nanoparticles with higher wave numbers.

From Figure 5 it is observed that with the increase in nanoparticle size the stability region decreases. This is because of the reason that for a fixed nanoparticle concentration in the pure base fluid, with the increase in nanoparticle size, aggregate volume fraction decreases. Therefore, with the increase of nanoparticle diameter the overall viscosity of nanofluid decreases, hence it destabilizes the flow.

In Figure 6 neutral curves have been plotted for Al_2O_3 − water nanofluid and air combination with respect to different volume fractions of nano-sized Al_2O_3 particles in water. It is observed that stable region increases on increasing the particle volume fraction in the base fluid. It is obvious as well because with the increase in nanoparticle volume fraction, the equivalent volume fraction which resulted from the nanolayer formed around the nanoparticle increases, and hence aggregate fraction increases which further increases the viscosity of the nanofluid, and therefore results in the stability in the fluid flow behavior.
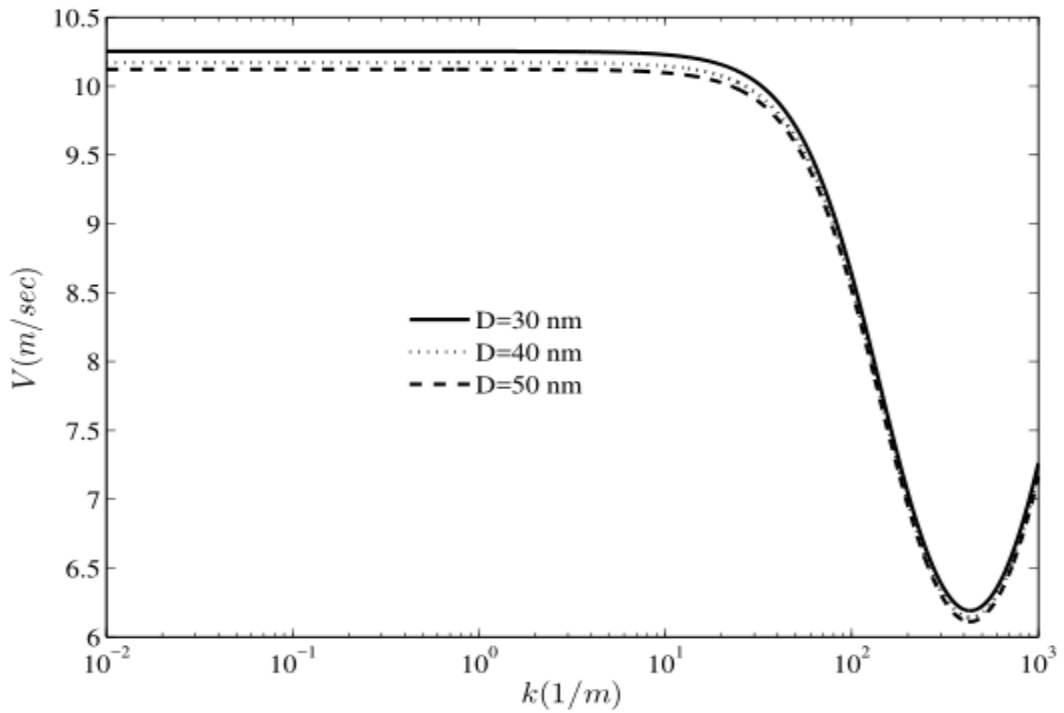
Figure 5: Water-based alumina for different diameters $\beta = 0.5, \varphi = 0.5$
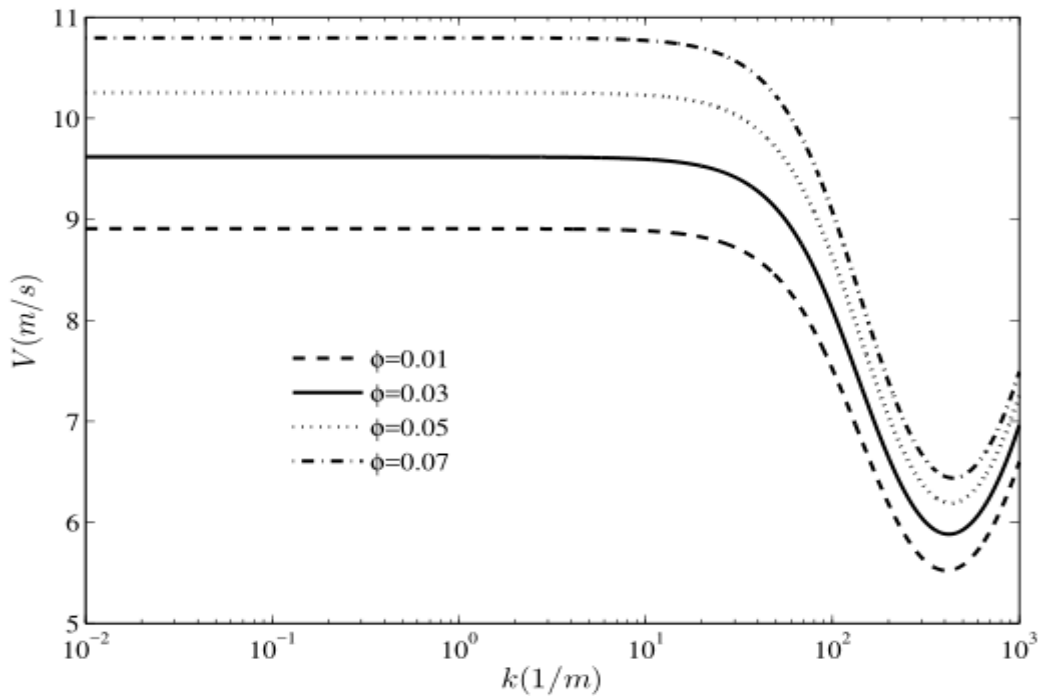

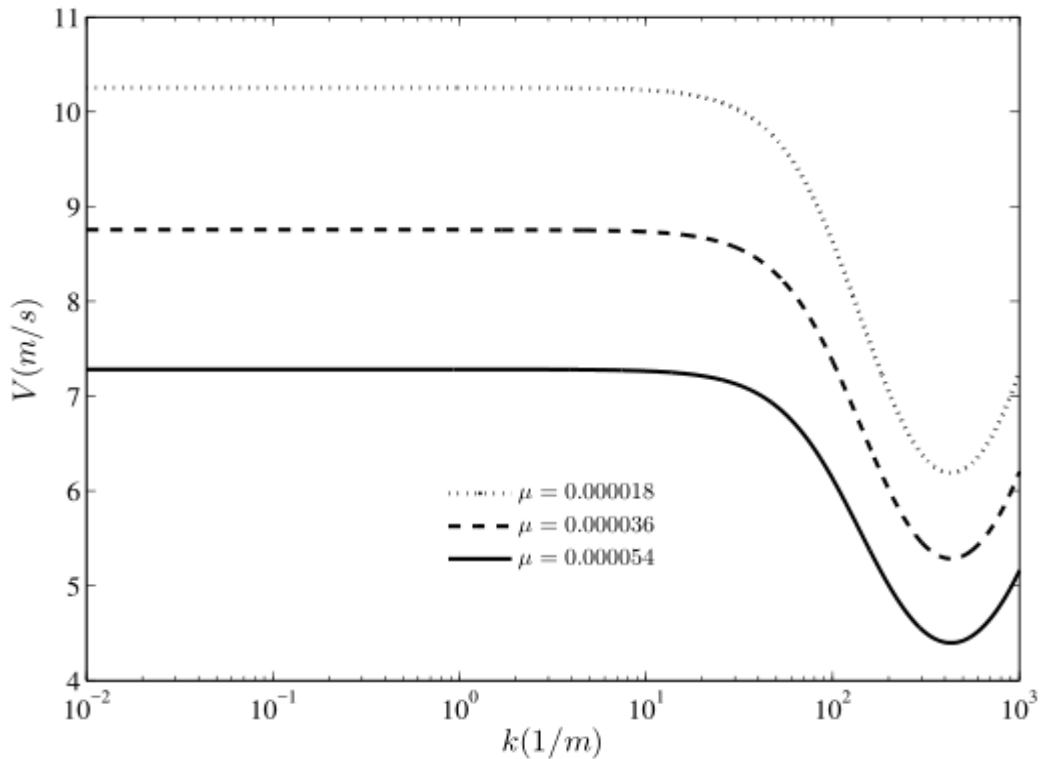Figure 6: water based Alumina for different $\varphi(\beta = 0.5)$

Figure 7: Water-basedaluminafor different viscosity of upper fluids$\beta = 0.5, \varphi = 0.5$

In Figure 7, Neutral curves have been plotted for different viscosity of upper fluids for water mixed with Aluminum Oxide & Air. It is observed that Viscosity stabilizes the system. The increase in viscosity induces extra viscous forces at the interface of two fluids and these viscous forces work to dampen the perturbations and the interface goes towards stability.

4.2. Sensitivity Analysis

The sensitivity of different parameters on $\hat{V}_{min}$ is performed by fitting a full quadratic regression model and a detailed Analysis of variance is performed. For this analysis Response Surface Method (RSM) is utilized. This method utilizes the concept of regression fit along with statistical analysis. The output is maximized with respect to the input variables. Further details of this method can be found in [28], [29], and [30].

Fully quadratic regression fit for "f" input variables used in RSM is given below:

$$Y = a_o + a_1 x_1 + \ldots + a_f x_f + a_{11}^2 x_1^2 + \ldots + a_{ff}^2 x_f^2 + a_{12} x_1 x_2 + \ldots + a_{f-1,f} x_{f-1} x_f \tag{32}$$

The above equation can also be represented as:

$$Y = fun(x_i, x_j) + \in$$

here, $\in$ represents the fitting error. The least square method is used to minimize the error for the best response surface fit.

To generate the response surface given by equation (32), the FCCD is used, which is shown in figure 8. The independent variables (inputs) are coded in the form of low (-1), medium (0), and high (1) values.

The total number of combinations of input variables needed to create the FCCD structure is calculated with the help of $N = 2^f + 2f + C$, where C represents the number of central points of the cubical structure. For the present study, the total number of input variables is 3, and for FCCD =6, which gives $N = 20$. The overall input variables combinations and the corresponding outputs (responses) are presented in table 2. To fit the model MiniTab software
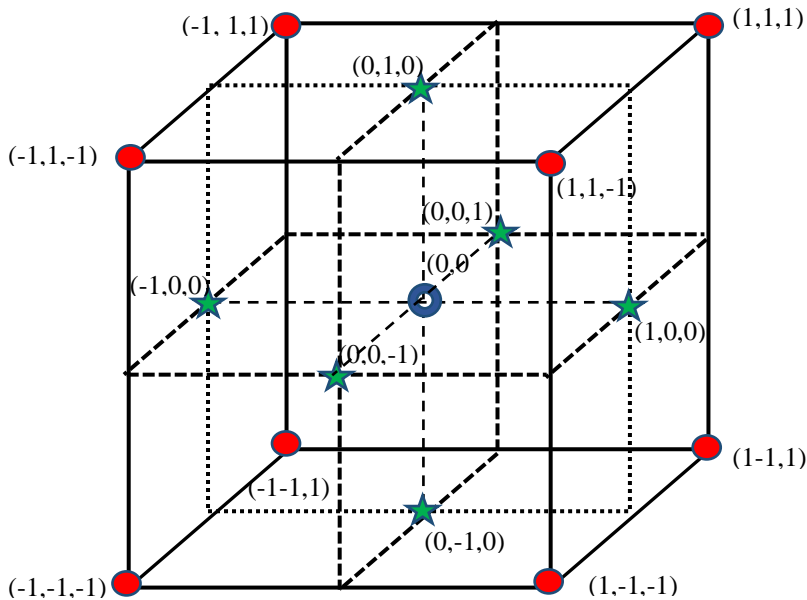
is used.

Figure8: Full factorial face-centered central composite design

To create the response, the surface of the input variables is considered in the below-given ranges.
$0.2 < \hat{h}_2 < 0.8, \quad 0.01 < \varnothing < 0.05, \quad and \quad 0.0010 < \hat{\rho} < 0.0012$
Considering all the possible combinations the coded input/output table for CCD is presented in Table 2.

Table 2: Input-output Table for CCD.

	Numerical experiment Serial no.	Coded Variable A (A is coded $\hat{h}_2$)	Coded Variable B (B is coded $\varnothing$)	Coded Variable C (C is coded $\hat{\rho}$)	Response/Output (1)$\hat{V}_{min}$
Corner points (2^f)	1	-1	-1	-1	0.4181
	2	1	-1	-1	0.4242
	3	-1	1	-1	0.4283
	4	1	1	-1	0.4332
	5	-1	-1	1	0.4343
	6	1	-1	1	0.4447
	7	-1	1	1	0.4487
	8	1	1	1	0.4566
Axial points ($2f$)	9	-1	0	0	0.4321
	10	1	0	0	0.4391
	11	0	-1	0	0.4358
	12	0	1	0	0.4441
	13	0	0	-1	0.4287
	14	0	0	1	0.4508
Repeated centre points(C)	15	0	0	0	0.4391
	16	0	0	0	0.4391
	17	0	0	0	0.4391
	18	0	0	0	0.4391
	19	0	0	0	0.4391
	20	0	0	0	0.4391

Quadratic Mathematical Model:

The important independent variables and their mutual interactions are identified by using the statistical "Pareto chart at $\alpha = 0.05$" given in Figure 9.
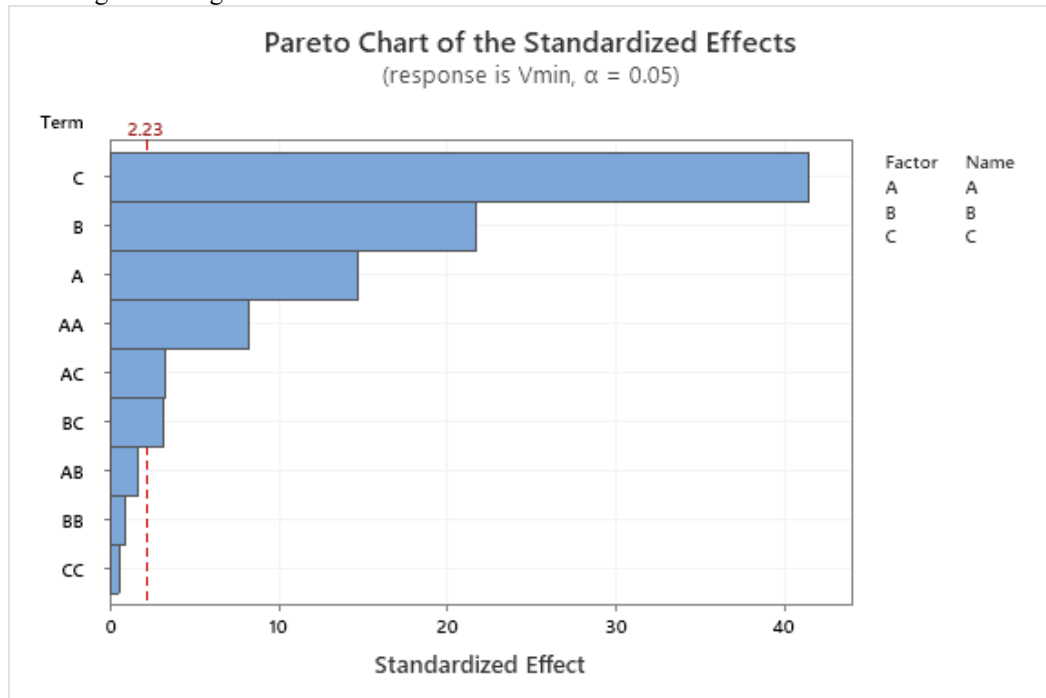

Figure 9: Pareto chart at $\alpha = 0.05$

Based on the significant parameters the fitted quadratic models for $\hat{V}_{min}$ is given in equations (33).

$$\hat{V}_{min} = 0.439258 + 0.003630\,A + 0.005380\,B + 0.010260\,C - 0.003895\,A^2 + 0.000913\,A*C + 0.000888\,B*C$$

(33)

Analysis of Variance (ANOVA):

To further confirm the validity of the equation (33), an Analysis of variance is utilized. The statistical significance of the terms in the regression equation is determined by computing the p-values using F-distribution. The detailed ANOVA is shown in Table 3. F-distribution and corresponding p-values are calculated for each term and at a 95% level of significance, the important parameters and corresponding interaction terms are identified.

Table 3: ANOVA Table for $\hat{V}_{min}$.

Source	DF	Adj SS	Adj MS	F-Value	P-Value	Comment
Model	9	0.001550	0.000172	281.76	0.000	*
Linear	3	0.001474	0.000491	803.81	0.000	*
A	1	0.000132	0.000132	215.59	0.000	Significant
B	1	0.000289	0.000289	473.56	0.000	Significant
C	1	0.001053	0.001053	1722.29	0.000	Significant
Square	3	0.000061	0.000020	33.46	0.000	*
A*A	1	0.000042	0.000042	68.27	0.000	Significant
B*B	1	0.000001	0.000001	0.93	0.358	Insignificant
C*C	1	0.000000	0.000000	0.29	0.601	Insignificant
2-Way Interaction	3	0.000015	0.000005	8.00	0.005	*

A*B	1	0.000002	0.000002	2.80	0.125	Insignificant
A*C	1	0.000007	0.000007	10.90	0.008	Significant
B*C	1	0.000006	0.000006	10.31	0.009	Significant
Error	10	0.000006	0.000001			
Lack-of-Fit	5	0.000006	0.000001	*	*	*
Pure Error	5	0.000000	0.000000			*
Total	19	0.001556				

The goodness of fitted quadratic models:

The goodness of fitted models is evaluated by computing the corresponding coefficients of determination. For $\hat{V}_{min}$ this value is obtained as 0.9961. Various error plots areanalyzed to validate the analysis further. These plots are shown in figure 10. These residual plots confirm the normality, independence, and randomness assumptions of the Analysis of Variance.
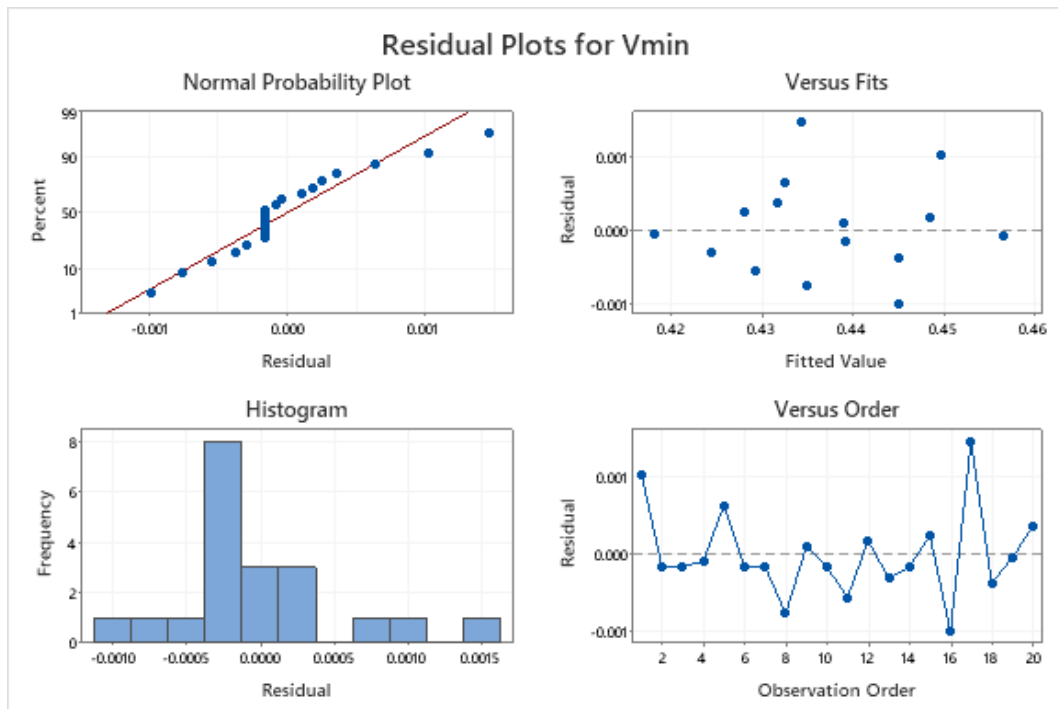

Figure 10: Residual plots for $\hat{V}_{min}$

Sensitivity Analysis:

The sensitivities of $\hat{V}_{min}$ on different parameters are obtained by partial differentiation of equations (33)with respect to the input parameters and are given in equations (33)-(38)

$$G\left(\hat{V}_{min}, A\right) = \frac{\partial \hat{V}_{min}}{\partial A} = 0.003630 - 0.007790\,A + 0.000913\,C \tag{34}$$

$$G\left(\hat{V}_{min}, B\right) = \frac{\partial \hat{V}_{min}}{\partial B} = 0.005380 + 0.000888\,C \tag{35}$$

$$G\left(\hat{V}_{min}, C\right) = \frac{\partial \hat{V}_{min}}{\partial C} = 0.010260\,C + 0.000913\,A + 0.000888\,B \tag{36}$$

In the present analysis, the sensitivities are analyzed by keeping B at medium value and changing the other variables from low to high values. The sensitivity plots for $\hat{V}_{min}$ are presented in Figures 11(a, b, c).In these figures,

the sensitivity is demonstrated using bar graphs. The bars in the positive direction show the positive sensitivity whereas the bars in the negative direction represent the negative sensitivity. The parameters A=-1, 0, 1, B=-1, 0, 1, and C= -1, 0, 1 are representing the coded values for the non-dimensional parameter $\hat{h}_2$=0.2, 0.5, 0.8, $\emptyset$=0.01, 0.03, 0.05 and $\hat{\rho}$=0.0010, 0.0011, 0.0012 respectively.

Figure 11a depicts that for the minimum value of A, the $\hat{V}_{min}$ is most sensitive to parameter A.

From Figure 11b, it is depicted that $\hat{V}_{min}$ is positively sensitive with respect to all the parameters A, B, and C, and the maximum sensitivity is observed for C, i.e. non-dimensional density parameter.

The sensitivities of $\hat{V}_{min}$ for the high value of A are plotted in Figure 11c. It is depicted that $\hat{V}_{min}$ is negatively sensitive to the parameter A, and the magnitude of this negative sensitivity decreases with increasing value of parameter C. Figure 10c also depicts that $\hat{V}_{min}$ has the highest positive sensitivity for parameter C.
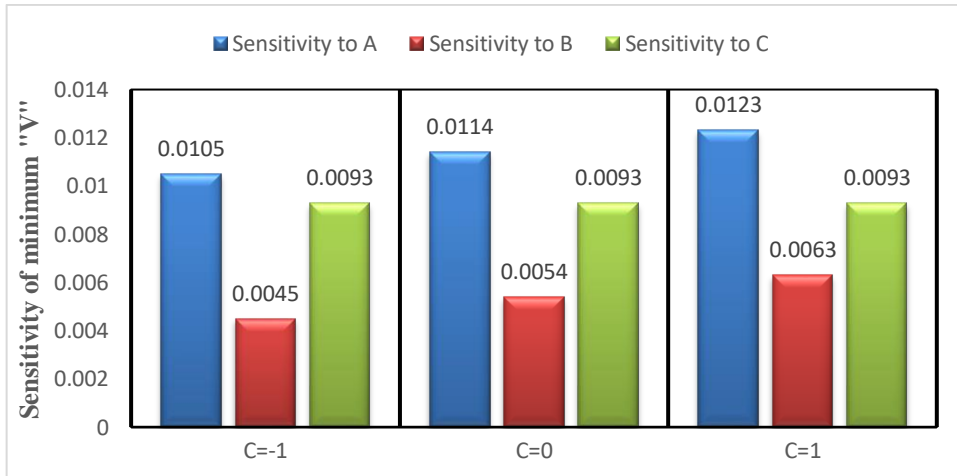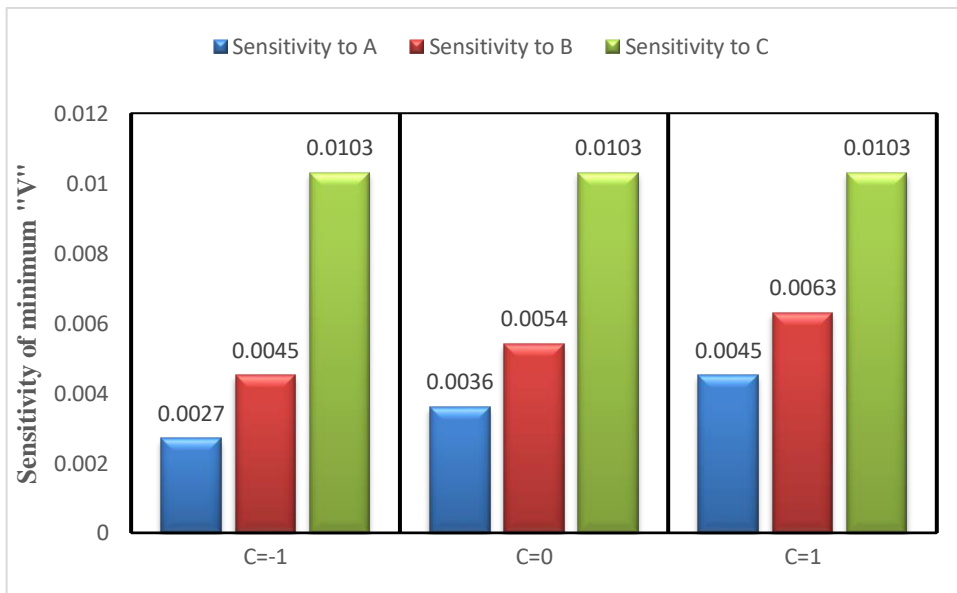

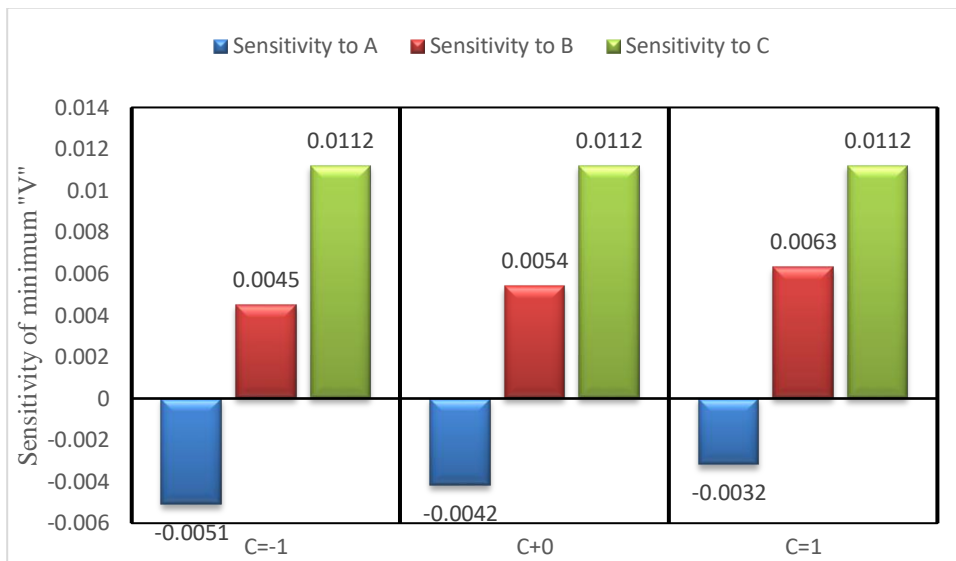Figure 11a: For A=-1

Figure 11b: For A=0

Figure 11c: For A=1

5. Conclusion

The Kelvin-Helmholtz instability at the interface of air and nano-fluid is considered in the present study. Stability Analysis and sensitivity analysis are discussed in this paper. Marginal stability in terms of relative velocity is presented. A minimum relative velocity is required for the instability to set in. sensitivity analysis has been done to study not only the effect of different parameters on the stability but also to study their combined effect. It has been observed that the particle size has a destabilizing effect. Nanoparticle volume fraction has to stabilize effect. Ethylene glycol-based Cupric oxide is the most stable of all nano-fluids that we have considered in this study. Sensitivity analysis using RSM has been discussed for critical velocity (Minimum velocity on the neutral curve). The nanofluid/air system demonstrates greater stability compared to the viscous liquid/air system. It is observed that the critical velocity consistently shows positive sensitivity to the density ratio, and the magnitude of these sensitivities remains constant across all cases. The critical velocity exhibits the highest positive sensitivity concerning the air thickness parameter, with this maximum sensitivity occurring when the air thickness is 1 and the densities of both fluids are equal.

References

[1]   Helmholtz, XLIII. On discontinuous movements of fluids, *The London, Edinburgh, and Dublin Philosophical Magazine and Journal of Science,* Vol. 36, No. 244, pp. 337-346, 1868.
[2]   W. Thomson, XLVI. Hydrokinetic solutions and observations, *The London, Edinburgh, and Dublin Philosophical Magazine and Journal of Science,* Vol. 42, No. 281, pp. 362-377, 1871.
[3]   P. Drazin, Kelvin–Helmholtz instability of finite amplitude, *Journal of Fluid Mechanics,* Vol. 42, No. 2, pp. 321-335, 1970.
[4]   S. Maslowe, R. Kelly, Finite-amplitude oscillations in a Kelvin-Helmholtz flow, *International Journal of Non-Linear Mechanics,* Vol. 5, No. 3, pp. 427-435, 1970.
[5]   A. H. Nayfeh, W. S. Saric, Non-linear kelvin–helmholtz instability, *Journal of Fluid Mechanics,* Vol. 46, No. 2, pp. 209-231, 1971.
[6]   M. Weissman, Nonlinear wave packets in the Kelvin-Helmholtz instability, *Philosophical Transactions of the Royal Society of London. Series A, Mathematical and Physical Sciences,* Vol. 290, No. 1377, pp. 639-681, 1979.
[7]   D. D. Joseph, T. Y. Liao, Potential flows of viscous and viscoelastic fluids, *Journal of Fluid Mechanics,* Vol. 265, pp. 1-23, 1994.

[8]   T. Funada, D. Joseph, Viscous potential flow analysis of Kelvin–Helmholtz instability in a channel, *Journal of Fluid Mechanics,* Vol. 445, pp. 263-283, 2001.

[9]   M. K. Awasthi, G. Agrawal, Viscous potential flow analysis of Kelvin–Helmholtz instability of cylindrical interface, *International Journal of Applied Mathematics and Computation,* Vol. 3, No. 2, pp. 131-138, 2011.

[10]   H. Kim, J. Padrino, D. Joseph, Viscous effects on Kelvin–Helmholtz instability in a channel, *Journal of fluid mechanics,* Vol. 680, pp. 398-416, 2011.

[11]   G. M. Moatimid, Y. M. Mohamed, A novel methodology in analyzing nonlinear stability of two electrified viscoelastic liquids, *Chinese Journal of Physics,* Vol. 89, pp. 679-706, 2024.

[12]   G. M. Moatimid, M. A. Mohamed, K. Elagamy, Nonlinear Kelvin-Helmholtz instability of a horizontal interface separating two electrified Walters' B liquids: A new approach, *Chinese Journal of Physics,* Vol. 85, pp. 629-648, 2023.

[13]   G. M. Moatimid, M. H. Zekry, N. S. Gad, Nonlinear EHD instability of a cylindrical interface between two walters B'fluids in porous media, *Journal of Porous Media,* Vol. 25, No. 3, 2022.

[14]   Z. Uddin, S. Harmand, S. Ahmed, Computational modeling of heat transfer in rotating heat pipes using nanofluids: A numerical study using PSO, *International Journal of Thermal Sciences,* Vol. 112, pp. 44-54, 2017.

[15]   Z. Uddin, S. Harmand, Natural convection heat transfer of nanofluids along a vertical plate embedded in porous medium, *Nanoscale research letters,* Vol. 8, pp. 1-19, 2013.

[16]   X.-Q. Wang, A. S. Mujumdar, A review on nanofluids-part II: experiments and applications, *Brazilian Journal of Chemical Engineering,* Vol. 25, pp. 631-648, 2008.

[17]   X.-Q. Wang, A. S. Mujumdar, A review on nanofluids-part I: theoretical and numerical investigations, *Brazilian journal of chemical engineering,* Vol. 25, pp. 613-630, 2008.

[18]   W. Yu, S. Choi, The role of interfacial layers in the enhanced thermal conductivity of nanofluids: a renovated Maxwell model, *Journal of nanoparticle research,* Vol. 5, pp. 167-171, 2003.

[19]   Gaganpreet, S. Srivastava, Viscosity of nanofluids: particle shape and fractal aggregates, *Physics and Chemistry of Liquids,* Vol. 53, No. 2, pp. 174-186, 2015.

[20]   G. M. Moatimid, M. A. Hassan, Convection instability of non-Newtonian Walter's nanofluid along a vertical layer, *Journal of the Egyptian Mathematical Society,* Vol. 25, No. 2, pp. 220-229, 2017.

[21]   G. M. Moatimid, M. A. Hassan, Linear instability of water–oil electrohydrodynamic nanofluid layers: Analytical and numerical study, *Journal of Computational and Theoretical Nanoscience,* Vol. 15, No. 5, pp. 1495-1510, 2018.

[22]   J. Ahuja, P. Girotra, Analytical and numerical investigation of Rayleigh–Taylor instability in nanofluids, *Pramana,* Vol. 95, pp. 1-12, 2021.

[23]   M. K. Awasthi, Z. Uddin, R. Asthana, Temporal instability of a power-law viscoelastic nanofluid layer, *The European Physical Journal Special Topics,* Vol. 230, pp. 1427-1434, 2021.

[24]   P. Girotra, J. Ahuja, D. Verma, Analysis of Rayleigh Taylor instability in nanofluids with rotation, *Algebra Control Opt Numer*, 2021.

[25]   J. Ahuja, P. Girotra, RAYLEIGH-TAYLOR INSTABILITY IN NANOFLUIDS THROUGH POROUS MEDIUM, *Journal of Porous Media,* Vol. 24, No. 8, 2021.

[26]   M. K. Awasthi, Dharamendra, D. Yadav, Temporal instability of nanofluid layer in a circular cylindrical cavity, *The European Physical Journal Special Topics,* Vol. 231, No. 13, pp. 2773-2779, 2022.

[27]   G. M. Moatimid, M. A. Hassan, M. A. Mohamed, Temporal instability of a confined nano-liquid film with the Marangoni convection effect: Viscous potential theory, *Microsystem Technologies,* Vol. 26, pp. 2123-2136, 2020.

[28]   Y. Han, KELVIN− HELMHOLTZ INSTABILITY OF A CONFINED NANO-LIQUID SHEET WITH THE EFFECTS OF HEAT ANDMASS TRANSFER ANDMARANGONI CONVECTION, *Atomization and Sprays,* Vol. 32, No. 1, 2022.

[29]   M. K. Awasthi, A. Kumar, N. Dutt, *Modeling Rayleigh-Taylor instability in nanofluid layers*, in: *Computational Fluid Flow and Heat Transfer*, Eds., pp. 249-262: CRC Press, 2024.

[30]   S. Agarwal, M. K. Awasthi, A. K. Shukla, Stability analysis of water-alumina nanofluid film at the spherical interface, *Proceedings of the Institution of Mechanical Engineers, Part E: Journal of Process Mechanical Engineering*, pp. 09544089221150733, 2023.

[31]   G. Leonzio, E. Zondervan, *Innovative application of statistical analysis for the optimization of CO2 absorption from flue gas with ionic liquid*, in: *Computer Aided Chemical Engineering*, Eds., pp. 151-156: Elsevier, 2019.

[32]   T. Mehmood, M. Ramzan, F. Howari, S. Kadry, Y.-M. Chu, Application of response surface methodology on the nanofluid flow over a rotating disk with autocatalytic chemical reaction and entropy generation optimization, *Scientific Reports,* Vol. 11, No. 1, pp. 4021, 2021/02/17, 2021.

[33]   H. Upreti, Z. Uddin, A. K. Pandey, N. Joshi, Sensitivity analysis for Sisko nanofluid flow through stretching surface using response surface methodology, 2023.

[34]   Z. Uddin, H. Hassan, S. Harmand, W. Ibrahim, Soft computing and statistical approach for sensitivity analysis of heat transfer through the hybrid nanoliquid film in rotating heat pipe, *Scientific Reports,* Vol. 12, No. 1, pp. 14983, 2022.

[35]   O. A. Bég, D. S. Espinoza, A. Kadir, M. Shamshuddin, A. Sohail, Experimental study of improved rheology and lubricity of drilling fluids enhanced with nano-particles, *Applied Nanoscience,* Vol. 8, pp. 1069-1090, 2018.

[36]   M. Shamshuddin, A. Saeed, S. Mishra, R. Katta, M. R. Eid, Homotopic simulation of MHD bioconvective flow of water-based hybrid nanofluid over a thermal convective exponential stretching surface, *International Journal of Numerical Methods for Heat & Fluid Flow,* Vol. 34, No. 1, pp. 31-53, 2024.

[37]   S. Salawu, E. Akinola, M. Shamshuddin, Entropy generation and current density of tangent hyperbolic Cu-C2H6O2 and ZrO2-Cu/C2H6O2 hybridized electromagnetic nanofluid: a thermal power application, *South African Journal of Chemical Engineering,* Vol. 46, pp. 1-11, 2023.